

Optimized Multiple Quantum MAS Lineshape Simulations in Solid State NMR

William J. Brouwer^{a,*} Michael C. Davis^a Karl T. Mueller^a

^a*Department of Chemistry, Pennsylvania State University*

Abstract

The majority of nuclei available for study in solid state Nuclear Magnetic Resonance have half-integer spin $I > 1/2$, with corresponding electric quadrupole moment. As such, they may couple with a surrounding electric field gradient. This effect produces anisotropic line broadening in spectra for distinct chemical species in polycrystalline solids. In Multiple Quantum Magic Angle Spinning (MQMAS) experiments, a second frequency dimension is created, devoid of quadrupolar anisotropy. As a result, the bary centers of peaks in the high resolution dimension are functions of isotropic quadrupole and chemical shifts alone. However, for complex materials, these parameters take on a stochastic nature due in turn to structural and chemical disorder. Lineshapes may still overlap in the isotropic dimension, complicating the task of assignment and interpretation. A distributed computational approach is presented here which permits optimal simulation of the MQMAS spectrum, generated by random variates from model distributions of isotropic chemical and quadrupole shifts. In this manner, local chemical environments for disordered materials may be characterized and via a re-sampling approach, error estimates for parameters produced.

Key words: Nuclear Magnetic Resonance, Multiple Quantum Magic Angle Spinning, OpenMP, Sobol sequence, quasi-random numbers, simulated annealing, distribution functions, quadrupole interaction.

1 Introduction

2 Since the discovery of Nuclear Magnetic Resonance (NMR), there has been
3 great interest in the study of quadrupolar nuclei. These nuclei have an electric
4 quadrupole moment Q which couples with a non-zero electric field gradient [8].

* Corresponding Author

Email address: `wjb19@psu.edu` (William J. Brouwer).

5 Depending on the magnitude of these quantities, the quadrupole interaction is
6 quite often the most significant perturbation to the Zeeman energy levels. At-
7 tention here is restricted to first and second order quadrupole effects, each of
8 which is proportional to a second rank tensor term $P_2(\theta)$ [41,36]. In addition,
9 the second order quadrupole perturbation is proportional to a fourth rank term
10 $P_4(\theta)$ ¹. These terms depend explicitly on the angle θ between crystallite orien-
11 tations and the static, applied magnetic field of NMR. As a result, anisotropic
12 frequency dependence is introduced, promoting overlap between lineshapes
13 arising from distinct chemical sites in powdered solids. Additionally, an ap-
14 preciable second order isotropic shift occurs; the bary center of quadrupole
15 lineshapes is subsequently changed from the chemically shifted value. The
16 characteristic features of quadrupole spectra provide valuable local bonding
17 information and hence extensive work has been devoted to both resolving
18 individual chemical sites, as well as lineshape simulation. With regard to res-
19 olution, the issue has been addressed over the course of time by a number of
20 experimental approaches. Early in the development of solid state NMR, Magic
21 Angle Spinning (MAS) [18] was proposed, which reduces or eliminates sec-
22 ond rank interaction terms and therefore broadening associated with the first
23 order quadrupole interaction. However, if the magnitude of the quadrupole
24 interaction is significant, spinning sideband manifolds arising from satellite
25 frequency transitions may still obscure spectra in one dimension [37]. Double
26 Rotation (DOR) [5] is an extension of the Magic Angle Spinning technique,
27 where by virtue of sample spinning at two angles, on the time average first and
28 second order quadrupole anisotropy are alleviated. In order to enhance reso-
29 lution beyond that available in one dimension, a natural extension was made
30 to two dimensional experiments [6] where quadrupolar nutation frequencies
31 (and thus underlying parameters) could be extracted via simulation. Dynamic
32 Angle Spinning (DAS) [33,32] is successful in eliminating the effects of both
33 second and fourth rank tensor terms, and thus also second order quadrupole
34 broadening. More recently, Multiple Quantum Magic Angle Spinning (MQ-
35 MAS) [2,47] and Satellite Transition Magic Angle Spinning (STMAS) [25,24]
36 have become popular owing to mechanical simplicity. These procedures in-
37 volve collecting data as a function of two independent time intervals in the
38 pulse sequence [51] under Magic Angle Spinning conditions. Within these ex-
39 periments, directly observable single quantum coherence frequency transitions
40 are correlated with multiple quantum transitions [62], which evolve between
41 pulses and are selected via an appropriate phase cycle, figure 1.

42 During data processing, a so-called ‘shearing transformation’ is applied af-
43 ter the Fourier transform in the direct dimension. This takes place before a
44 Fourier transform in the second dimension, in order to create a high resolu-
45 tion spectrum in the indirect dimension, devoid of anisotropy. Alternatively,
46 a high resolution axis may be created during the experimental acquisition us-

¹ Relevant expressions are listed in Appendix A

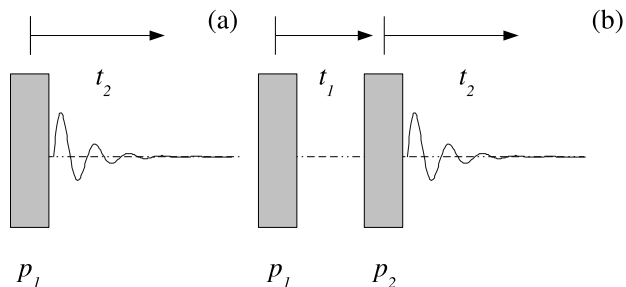


Fig. 1. (a) Schematic of a 1D NMR experiment; p_1 is the pulse duration, and the free induction decay is recorded during the acquisition time period t_2 . Coherences which have a change in magnetic quantum number Δm equal to ± 1 are detected, as supported by the electric dipole selection rule. (b) Schematic of a 2D NMR experiment; acquisition takes place during t_2 and time period t_1 is varied to create a second, indirect dimension. Multiple quantum $\Delta m \neq \pm 1$ as well as single quantum coherences evolve during this period. Ultimately, a particular coherence transfer pathway (CTP) is selected in an MQMAS experiment via a phase table; phases of pulses are varied in a prescribed manner to ensure the desired CTP amplitude is a maximum.

47 ing the split- t_1 method [14]. Figure 2 displays the ^{27}Al MQMAS spectrum
 48 of the large-pore aluminophosphate VPI-5 as a contour plot, alongside the
 49 MAS (F2) frequency dimension projection. Clearly resolved are two distinct
 50 chemical sites in the tetrahedral coordination region of the aluminum spectral
 51 window.

52 From the bary centre of peaks along the high resolution axis, isotropic shifts are
 53 deduced which are a function of both isotropic chemical and quadrupole shifts.
 54 In turn, the isotropic quadrupole shift is a function of both the quadrupole
 55 coupling constant C_q and asymmetry parameter η . The importance of these
 56 quantities lies in the fact that they are directly related to the electric field
 57 gradient tensor, and thus the details of the local bonding environment. In
 58 order to unequivocally determine both C_q and η , simulation of experimental
 59 spectra is necessary. Work in this area was initially devoted to static line-
 60 shapes [11,52] and has since been extended to spinning solids. Several exam-
 61 ples of the latter include extraction of quadrupolar parameters using spinning
 62 sideband manifolds [30,1] and the use of the stochastic Liouville von-Neumann
 63 equation to incorporate molecular motion [27]. In the last decade, simulation

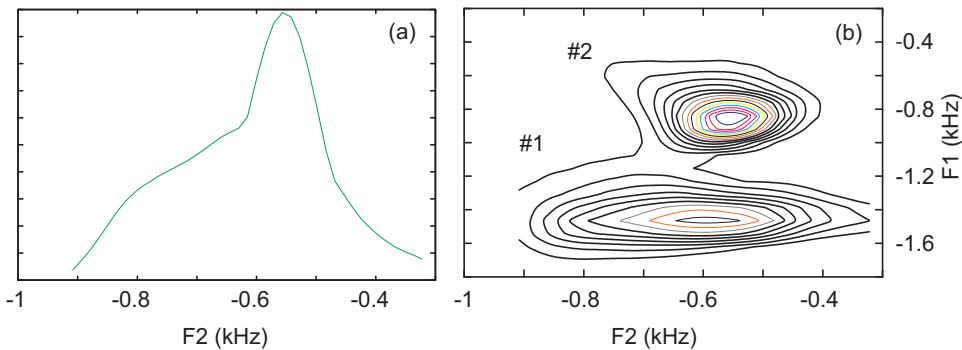


Fig. 2. (a) ^{27}Al MAS spectrum of tetrahedral region within VPI-5 (b) Contour plot of MQMAS spectrum of same compound; clearly resolved are two chemical sites with distinctive lineshapes and hence local environments.

64 tools including SIMPSON [35] and GAMMA [54] have been created. Cal-
 65 culations performed by these packages can take into account radio frequency
 66 pulse powers and durations, time delays, expected NMR parameters and other
 67 variables to provide a system response. There also exists lineshape modeling
 68 tools such as DMFIT [15] which provides simulation capabilities for a large
 69 variety of experiments and interactions. In the case of disordered chemical
 70 environments [23,9,57,56], calculations of powdered lineshapes for MQMAS
 71 becomes a formidable task. This is due to the fact that parameters relevant
 72 to simulation take on a distributed nature [49,22]. Whether using a high level
 73 of theory, inversion methods [67], or the use of table-lookup in calculating
 74 powder patterns, computational demands become excessive. The focus of this
 75 paper is devoted to the optimized simulation of multiple quantum magic an-
 76 gle spinning spectra, in the presence of low to significant disorder. This is
 77 accomplished using quasi-random numbers sampled from model distributions
 78 of isotropic chemical shift and quadrupole coupling constant. Simulated an-
 79 nealing is used to optimize the non-convex cost function. In distinction to
 80 spectrum-inversion approaches [19], the method proposed here also gives in-
 81 sight into the asymmetry parameter and is highly amenable to distributed
 82 computing [26].

83 2 Theory

84 2.1 Quadrupole Interaction

85 The density operator is a popular means of describing experimental NMR. The
 86 matrix representation of this operator in a particular basis is diagonalized
 87 and the time evolution propagated using an average Hamiltonian [61]. The
 88 important assumption in this approach is the synchronization of the Magic

89 Angle Spinning (MAS) speed with evolution periods in the pulse sequence.
 90 A more general theory for time-dependent Hamiltonians is given via Floquet
 91 theory [7,59,55] and will not be treated here. The quadrupole interaction in
 92 terms of irreducible tensor operator notation [39,40,53] may be expressed as:

$$93 \quad \mathcal{H}_Q = N_Q \sum_{u=-2}^2 (-1)^u V_{2,-2} K^{(2,u)}$$

$$94 \quad \text{where } N_Q = \frac{eQ}{2I(2I-1)\hbar} \quad (1)$$

95 Tensor V contains electric field gradient terms, and tensor K spin angular
 96 momentum operators; expressions for these are given in appendix A. It is as-
 97 sumed for the remainder of this work that the quadrupole interaction may be
 98 treated as a weak perturbation on the Zeeman levels. One begins by consid-
 99 ering the time evolution of the operator in the interaction representation (ie.,
 100 the rotating frame):

$$101 \quad H_Q(t) = \exp(iH_z t) H_Q \exp(-iH_z t)$$

$$102 \quad = N_Q \sum_{u=-2}^2 (-1)^u V_{2,-u} K^{(2,u)} \exp(-iu\omega_0 t), \quad (2)$$

103 where ω_0 is the Larmor frequency. The Magnus expansion [38] is employed
 104 in order to find the average value of the Hamiltonian, assuming that the
 105 Hamiltonian may be considered piece-wise constant during short time inter-
 106 vals. Ignoring highly oscillating and non-secular terms (retaining only those
 107 that commute with the Zeeman Hamiltonian), one finds to first and second
 108 order for the quadrupole interaction:

$$109 \quad H_Q^{(1)} = \frac{1}{t_L} \int_0^{t_L} H_Q(t) dt = N_Q \frac{1}{\sqrt{6}} [3I_z^2 - I(I+1)] V_{2,0} \quad (3)$$

$$110 \quad H_Q^{(2)} = \frac{-i}{2t_L} \int_0^{t_L} dt \int_0^t dt' [H_Q(t), H_Q(t')] =$$

$$111 \quad \frac{-N_Q^2}{\omega_0} \left(\frac{1}{2} V_{2,-1} V_{2,1} [4I(I+1) - 8I_z^2 - 1] \right.$$

$$112 \quad \left. + \frac{1}{2} V_{2,-2} V_{2,2} [2I(I+1) - 2I_z^2 - 1] \right) I_z \quad (4)$$

113 For the purposes of determining frequency shifts, these expressions are sim-
 114 plified using higher rank tensors e.g.,

$$\begin{aligned}
 115 \quad H_Q^{(2)} &= \frac{-N_Q^2}{\omega_0} \left(\frac{1}{70} \sqrt{7} W_{4,0} [17L^{(3,0)} - 6L^{(1,0)}] \right. \\
 116 \quad &\left. + \frac{1}{\sqrt{35}} W_{2,0} [3L^{(3,0)} + L^{(1,0)}] - \frac{1}{10} \sqrt{2} W_{0,0} [3L^{(3,0)} - 4L^{(1,0)}] \right) \quad (5)
 \end{aligned}$$

117 The tensor W contains components of the electric field gradient, whilst tensor
 118 L is a function of spin operators. Explicitly, the tensor W is related to the
 119 tensor V via the Clebsch-Gordon coefficients,

$$120 \quad W_{j,M} = \sum_{m_1, m_2} \langle j_1 j_2 m_1 m_2 | JM \rangle V_{j_1, m_1} V_{j_2, m_2} \quad (6)$$

121 and the L are given by:

$$122 \quad L^{(1,0)} = \frac{1}{5} \sqrt{10} [I(I+1) - \frac{3}{4}] I_z \quad (7)$$

$$123 \quad L^{(3,0)} = \frac{1}{5} \sqrt{10} [3I(I+1) - 5I_z^2 - 1] I_z \quad (8)$$

124 The latter are not normalized; in terms of normalized tensor operators $P^{(1,0)}$
 125 and $P^{(3,0)}$ one may write:

$$126 \quad L^{(1,0)} = \sqrt{\frac{2}{5}} [I(I+1) - \frac{3}{4}] P^{(1,0)} \quad (9)$$

$$127 \quad L^{(3,0)} = -2P^{(3,0)} \quad (10)$$

128 Therefore

$$\begin{aligned}
 129 \quad H_Q^{(2)} &= \frac{-N_Q^2}{\omega_0} \left(\frac{-17}{5\sqrt{7}} W_{4,0} P^{(3,0)} - \frac{3}{35} \sqrt{\frac{16}{5}} [I(I+1) - \frac{3}{4}] \right. \\
 130 \quad &\times W_{4,0} P^{(1,0)} - \frac{6}{\sqrt{35}} W_{2,0} P^{(3,0)} + \frac{\sqrt{14}}{35} [I(I+1) - \frac{3}{4}] \\
 131 \quad &\times W_{2,0} P^{(1,0)} + \frac{3\sqrt{2}}{5} W_{0,0} P^{(3,0)} + \frac{4}{5\sqrt{5}} [I(I+1) - \frac{3}{4}] W_{0,0} P^{(1,0)} \left. \right) \quad (11)
 \end{aligned}$$

132 If one denotes distinct energy levels by r, c , then the shift to the standard
 133 Zeeman frequency may be determined as,

$$134 \quad \omega_{r,c} = \langle r | (H_Q^{(1)} + H_Q^{(2)}) | r \rangle - \langle c | (H_Q^{(1)} + H_Q^{(2)}) | c \rangle$$

135 which is the sum of first and second order contributions:

$$136 \quad \omega_{r,c}^{(1)} + \omega_{r,c}^{(2)} \quad (12)$$

137 To first order, the shift is:

$$138 \quad \omega_{r,c}^{(1)} = N_Q \sqrt{\frac{3}{2}} (r^2 - c^2) V_{2,0}, \quad (13)$$

139 which for a symmetric transition ($r = -c$) is zero. To second order:

$$140 \quad \omega_{r,c}^{(2)} =$$

$$141 \quad \frac{-N_Q^2}{\omega_0} (r - c) \left\{ \frac{1}{70} \sqrt{\frac{35}{2}} W_{4,0} A^{(4)} + \frac{1}{28} \sqrt{14} W_{2,0} A^{(2)} - \frac{1}{\sqrt{5}} W_{0,0} A^{(0)} \right\} \quad (14)$$

142 where expressions for constants A , which depend upon I, r, c , are given in
143 appendix A.

144 2.1.1 Static Crystal

145 It is convention to express frequencies in terms of the principal axis system,
146 the frame of reference where the tensor of interest is diagonal. Referring to
147 figure 3, the transformation for $V_{2,0}$ from the principal axis system is rather
148 simple in the case of a static single crystal:

$$149 \quad V_{2,0} = \sum_{u=-2}^2 V_{2,u}^{\text{PAS}} D_{u,0}^{(2)}(\alpha, \beta, \phi) =$$

$$150 \quad = \frac{1}{2} \sqrt{6} e q \left[\frac{1}{2} (3 \cos^2 \beta - 1) + \frac{1}{2} \eta \sin^2 \beta \cos 2\alpha \right], \quad (15)$$

151 where D is the Wigner rotation matrix. One may then write the 1st order
152 quadrupole interaction as:

$$153 \quad H_Q^{(1)} = \frac{1}{4} (3I_z^2 - I(I+1)) \Omega_Q [3 \cos^2 \beta - 1 + \eta \sin^2 \beta \cos 2\alpha] \quad (16)$$

154 with

$$155 \quad \Omega_Q = e q N_Q = \frac{e^2 q Q}{2I(2I-1)\hbar} = \frac{C_q}{2I(2I-1)}$$

156 Therefore, apart from orientation angles, quadrupole frequencies are com-
157 pletely specified in terms of parameters η and C_q , which are sufficient to de-
158 scribe the electric field gradient tensor, since in the PAS the tensor is diagonal

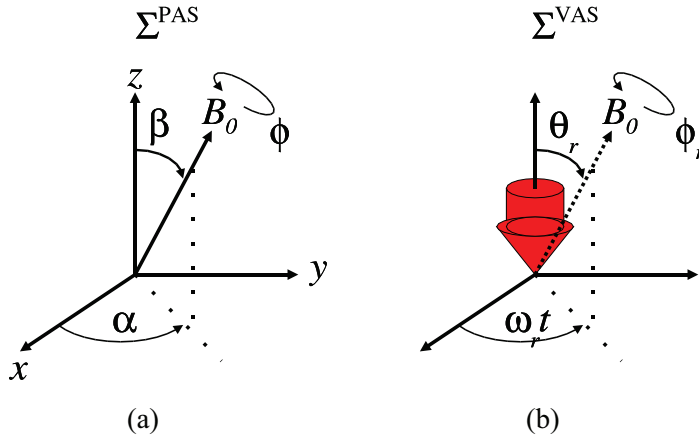


Fig. 3. Euler angles for: (a) the Principal Axis System (PAS) in the crystal frame (b) VAS/rotor relationship to static magnetic field B_0 .

159 and satisfies Laplace's equation. Tensor components $W_{4,0}$, $W_{2,0}$ and $W_{0,0}$ of the
 160 electric field gradient transform as;

$$161 \quad W_{2x,0} = \sum_{u=-x}^x W_{2x,2u}^{\text{PAS}} D_{2u,0}^{(2x)}(\alpha, \beta, \phi) \quad (17)$$

162 Hence for the second order quadrupole frequency:

$$163 \quad w_{r,c}^{(2)} = -\frac{r-c}{2\omega_0} \Omega_Q^2 \sum_k^{0,1,2} A^{(2k)}(I, r, c) \sum_{u=-k}^k B_{2k,2u}(\eta) D_{2u,0}^{(2k)}(\alpha, \beta, \phi) \quad (18)$$

164 with

$$\begin{aligned} B_{0,0}(\eta) &= -\frac{1}{5}(\eta^2 + 3), & B_{2,0}(\eta) &= \frac{1}{14}(\eta^2 - 3), \\ 165 \quad B_{2,\pm 2}(\eta) &= \frac{1}{14}\eta\sqrt{6}, & B_{4,0}(\eta) &= \frac{1}{140}(\eta^2 + 18), \\ B_{4,\pm 2}(\eta) &= \frac{3}{140}\eta\sqrt{10}, & B_{4,\pm 4}(\eta) &= \frac{1}{4\sqrt{70}}\eta^2 \end{aligned}$$

166 2.1.2 Magic Angle Spinning

167 Referring again to figure 3, in performing sample or variable angle spinning
 168 (VAS) at angle θ_r to the static field, with angular velocity ω_r , an additional
 169 step in transforming between PAS and the rotor frame is necessary:

$$170 \quad V_{2,u}^{\text{VAS}} = \sum_{j=-2}^2 V_{2,j}^{\text{PAS}} D_{j,u}^{(2)}(\alpha, \beta, \phi), \quad (19)$$

$$171 \quad V_{2,0} = \sum_{u=-2}^2 V_{2,u}^{\text{VAS}} D_{u,0}^{(2)}(\omega_r t, \theta_r, \phi_r) \quad (20)$$

172 For this case, the first order Quadrupole Interaction:

$$173 \quad \omega_{r,c}^{(1)\text{VAS}} =$$

$$174 \quad N_Q \frac{1}{2} \sqrt{6} (r^2 - c^2) \sum_{u=-2}^2 D_{u,0}^{(2)}(\omega_r t, \theta_r, \phi_r) \sum_{j=-2}^2 V_{2,j}^{\text{PAS}} D_{j,u}^{(2)}(\alpha, \beta, \phi) \quad (21)$$

175 Similarly, in determining the second order shift, one finds:

$$176 \quad W_{2x,u}^{\text{VAS}} = \sum_{j=-x}^x W_{2x,2j}^{\text{PAS}} D_{2j,u}^{(2x)}(\alpha, \beta, \phi) \quad (22)$$

$$177 \quad W_{2x,0} = \sum_{u=-2x}^2 x W_{2x,u}^{\text{VAS}} D_{u,0}^{(2x)}(\omega_r t, \theta_r, \phi_r) \quad (23)$$

178 and hence:

$$179 \quad \omega_{r,c}^{(2)\text{VAS}} = -\frac{r-c}{2\omega_0} \Omega_Q^2 \sum_{x=0}^2 A^{(2x)}(I, r, c) \times$$

$$180 \quad \sum_{u=-2x}^{2x} D_{u,0}^{(2x)}(\omega_r t, \theta_r, \phi_r) \sum_{j=-x}^x B_{2x,2j}(\eta) D_{2j,u}^{(2x)}(\alpha, \beta, \phi) \quad (24)$$

181 Now $D_{u,0}^{(2x)}$ is proportional to $\exp(-iu\omega_r t)$ and thus spinning sidebands are
 182 observed in the frequency domain. In the high spinning speed approximation,
 183 one assumes that the only non-zero term is for $u = 0$, thus:

$$184 \quad \omega_{r,c}^{(1)\text{VAS}'} = \nu_Q \frac{1}{2} \sqrt{6} (r^2 - c^2) d_{0,0}^{(2)}(\theta_r) \sum_{j=-2}^2 V_{2,j}^{\text{PAS}} D_{j,0}^{(2)}(\alpha, \beta, \phi) \quad (25)$$

$$185 \quad \omega_{r,c}^{(2)\text{VAS}'} = -\frac{r-c}{2\omega_0} \Omega_Q^2 \sum_{x=0}^2 A^{(2x)}(I, r, c) d_{0,0}^{(2x)}(\theta_r) \times$$

$$186 \quad \sum_{j=-x}^x B_{2x,2j}(\eta) D_{2j,0}^{(2x)}(\alpha, \beta, \phi) \quad (26)$$

$$187 \quad = -\frac{r-c}{2\omega_0} \Omega_Q^2 \{A^{(0)}(I, r, c) B_{0,0}(\eta) + A^{(2)}(I, r, c) d_{0,0}^{(2)}(\theta_r) [B_{2,0}(\eta) d_{0,0}^{(2)}(\beta)$$

$$188 \quad + 2B_{2,2}(\eta) d_{2,0}^{(2)}(\beta) \cos 2\alpha] + A^{(4)}(I, r, c) d_{0,0}^{(4)}(\theta_r) [B_{4,0}(\eta) d_{0,0}^{(4)}(\beta)$$

$$189 \quad + 2B_{4,2}(\eta) d_{2,0}^{(4)}(\beta) \cos 2\alpha + 2B_{4,4}(\eta) d_{4,0}^{(4)}(\beta) \cos 4\alpha]\} \quad (27)$$

190 Further, under the Magic Angle Spinning condition of $P_2(\cos \theta_r) = 0$, there
 191 remains for the first and second order quadrupole interactions:

$$192 \quad \omega_{r,c}^{(1)\text{fast MAS}} = 0, \quad (28)$$

$$193 \quad \omega_{r,c}^{(2)\text{fast MAS}} =$$

$$194 \quad \omega_{r,c}^{\text{iso}} - \frac{r-c}{2\omega_0} \Omega_Q^2 \{A^{(0)}(I, r, c)B_{0,0}(\eta) + A^{(4)}(I, r, c)[B_{4,0}(\eta)d_{0,0}^{(4)}(\beta) +$$

$$195 \quad 2B_{4,2}(\eta)d_{2,0}^{(4)}(\beta) \cos 2\alpha + 2B_{4,4}(\eta)d_{4,0}^{(4)}(\beta) \cos 4\alpha]P_4(\cos \theta_m)\}. \quad (29)$$

196 This expression² will be used to describe frequencies in the direct dimension
 197 for which $r - c = -1$ as well as the indirect dimension. The MQMAS experi-
 198 ments performed in this work use the triple quantum transition, ie., $r - c = 3$.

199 2.2 Lineshape Simulation and Optimization

200 Since the introduction of MQMAS experiments, there have been significant
 201 improvements in excitation efficiency and coherence transfer using Double
 202 Frequency Sweep (DFS) [4,3] and Fast Amplitude Modulation [47,48]. The
 203 discovery of the rotatory resonance phenomena has been exploited particu-
 204 larly for low gamma nuclei [65,60] and there have been improvements made
 205 in sensitivity based around the inclusion of signal intensity from additional
 206 coherence transfer pathways [64,43]. The Z-filter [28] method ensures that
 207 amplitudes for echo and anti-echo pathways are co-added with equal inten-
 208 sity under States [17] acquisition, providing after phase correction a purely
 209 absorptive 2-D spectra. Therefore, using the second order perturbation theory
 210 expression for multiple quantum transition frequencies given in eq. 29, one
 211 may model the general 2D correlation spectrum between the $r \leftrightarrow c$ quan-
 212 tum transition (indirect frequency dimension) and central transition (direct
 213 frequency dimension $r - c = -1$) as [34,13,8]:

$$214 \quad F(f1, f2) = (1 - \epsilon) \frac{\lambda_1}{\lambda_1^2 + (f1 - f1_m)^2} \frac{\lambda_2}{\lambda_2^2 + (f2 - f2_m)^2}$$

$$215 \quad + \epsilon \frac{1}{2\pi\lambda_1\lambda_2} e^{\left(\frac{-(f1-f1_m)^2}{2\lambda_1^2} + \frac{-(f2-f2_m)^2}{2\lambda_2^2}\right)} \quad (30)$$

216 Where $2\pi f1_m = \omega_{r,c}^{(2)}$ and $2\pi f2_m = \omega_{-1}^{(2)}$ are the indirect and direct second
 217 order quadrupole frequency expressions. This model is pertinent to the dipole

² The isotropic chemical shift δ_{iso}^{cs} is implicit within equation 29; $\omega_{r,c}^{\text{iso}} = (r-c)\delta_{iso}^{cs}\omega_0$

Table 1
Powder averaging schemes

Method	α	β	w_j
Planar Grid	$\frac{2\pi k}{N_\alpha}$	$\frac{\pi(j+0.5)}{N_\beta}$	$\sin(\beta_j)$
Spherical Grid	$\frac{2\pi k}{N_\alpha}$	$\arccos\left(1 - \frac{2j+1}{N_\beta}\right)$	1
Planar ZCW	$\frac{2\pi(jM_z \bmod N_z)}{N_z}$	$\frac{(j+0.5)\pi}{N_z}$	$\sin(\beta_j)$
Spherical ZCW	$\frac{2\pi(jM_z \bmod N_z)}{N_z}$	$\arccos\left(1 - \frac{2j+1}{N_z}\right)$	1

218 broadened lineshape (broadening factors λ_1, λ_2) of a single crystallite orien-
 219 tation with unique isotropic chemical shift δ_{iso}^{cs} , asymmetry parameter η and
 220 quadrupole coupling constant C_q . As such, it provides a suitable kernel for a
 221 more general lineshape intensity function, weighted by crystallite angle distri-
 222 bution $G(\alpha, \beta)$ and probability density $P(\delta_{cs}^{iso}, C_q, \eta)$:

$$223 \quad I(f1, f2) =$$

$$224 \quad \sum_j^L \mathcal{A}_j \int_{\delta_{cs}^{iso}, C_q, \eta} \int_{\alpha, \beta} P_j(\delta_{cs}^{iso}, C_q, \eta) G(\alpha, \beta) F_j(f1, f2) d[\alpha, \beta] d[\delta_{cs}^{iso}, C_q, \eta] \quad (31)$$

225 where L is the number of chemical sites and \mathcal{A}_j the individual site amplitude.
 226 There are two aspects to a numerical evaluation of this expression, including
 227 powder averaging over the crystallite orientations specified by angles α and
 228 β . In addition, contributions to the overall spectrum from random variates
 229 C_q, δ_{iso}^{cs} , and η are weighted by a multi-variate probability distribution function.
 230 Powder averaging in magnetic resonance is an example of a problem in broader
 231 quantum mechanics, evaluating integrals over the unit sphere [21,20]. There
 232 exists several reviews in the literature with regard to powder averaging in
 233 magnetic resonance [50,46]. It is assumed that the equally probable crystallite
 234 orientations within a powder have been equally irradiated. Table one lists
 235 various schemes for performing powder averaging under these assumptions,
 236 where the integral over angles is replaced by a sum:

$$237 \quad \bar{F}(f1, f2) = \frac{\sum_i^N w_i F_i(\alpha, \beta)}{\sum_i^N w_i} \quad (32)$$

238 with various choices for weights w_i and angles α, β .

239

240 In the Planar grid or Alderman-Solum-Grant scheme [16], as well as for the
 241 Spherical Grid method, α and β are varied independently with N_α and N_β
 242 steps and $k = 0 \dots N_\alpha - 1, j = 0 \dots N_\beta - 1$. For the Zaremba-Conroy-Wolfsberg
 243 method [66,12,63], N_z and M_z are chosen to satisfy $M_z = F(m)$ and $N_z =$
 244 $F(m + 2)$, where $F(m)$ the m th Fibonacci number. The latter method has

245 been employed for the simulations in this work, and is anticipated to be op-
 246 timal for fast MAS and few crystallite contributions [46]. To incorporate the
 247 multivariate distribution in isotropic chemical shift and quadrupole param-
 248 eters, variables are sampled from a model distribution and a Monte Carlo
 249 simulation performed. In general, statistical distributions may be symmetric
 250 or asymmetric. The nature of the model distribution used in the simulation
 251 is directly related to the underlying chemical and/or structural disorder. Tra-
 252 ditional random number generators which create variates according to dis-
 253 tributions such as these are usually one of two types. They may be of the
 254 acceptance/rejection type, or rely on transformations of the uniform distri-
 255 bution, eg., the Box-Muller method for normal-distributed variables [45]. The
 256 latter was used here for ease of adaptation to a parallel programming envi-
 257 ronment. By creating variates after this fashion and converting the integral of
 258 eq. 31 to a summation, the integral is solved via a Monte Carlo approach. By
 259 the law of large numbers, Monte Carlo approximations converge to the true
 260 value in the limit as the samples N approach infinity. In reality, convergence is
 261 slow, and the error in using pseudo random numbers is $O(N^{-1/2})$. This situa-
 262 tion is improved via using quasi-random numbers such as the Sobol sequence,
 263 which have an error $O((\log N)^k N^{-1})$ for k dimensions [42]. For the purposes
 264 of this work, attention is restricted to the multi-variate normal distribution
 265 with density:

$$266 \quad p(x_1, \dots, x_n) = \frac{1}{(2\pi)^n |\Sigma|^{1/2}} \exp\left(-\frac{1}{2}(x - \mu)^T \Sigma^{-1}(x - \mu)\right) \quad (33)$$

267 where random variates x_1, \dots, x_n may represent quadrupole coupling constant
 268 C_q , asymmetry parameter η and isotropic chemical shift δ_{iso}^{cs} parameters (ie.,
 269 $n = 3$). Other symbols have their usual meaning; Σ is the covariance matrix
 270 with determinant $|\Sigma|$ and μ is the vector of mean values. There is a well estab-
 271 lished method for generating normally distributed variates which is employed
 272 here, specifically:

- 273 (1) The Cholesky decomposition of $AA^T = \Sigma$ is calculated, providing matrix
- 274 A .
- 275 (2) A vector Z of normal random variates are created via the Box-Muller
- 276 transform
- 277 (3) Multivariate parameters X with the desired properties are generated from
- 278 $X = \mu + AZ$

279 For the remainder of this work, attention is restricted to bi-variate distribu-
 280 tions in C_q and δ_{iso}^{cs} , parametrized by $\mu_x, \sigma_x, \mu_y, \sigma_y, \rho$, using single values of
 281 asymmetry parameter η per chemical site. Using the theory outlined thus far,
 282 an experimental spectrum may be simulated and attempts made to optimize
 283 the simulation parameters. Figure 4 is a plot of the cost function obtained by
 284 varying only chemical shifts in a fit to the two site, VPI-5 tetrahedral region.

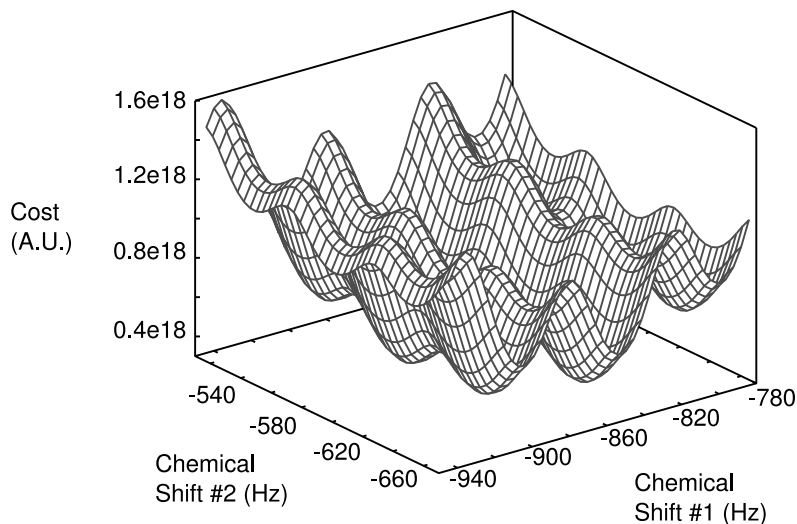


Fig. 4. Cost function, sum of squared difference between simulated and experimental VPI-5 MQMAS spectrum, as a function of the two isotropic chemical shifts

285 The global minima is toward the center of the plot, within a larger area
 286 containing local minima. Simulated annealing [31] is a stochastic method for
 287 global optimization suited to non-convex cost functions. The method is analo-
 288 gous to the metallurgical process of annealing. The application to the current
 289 problem ensures that the iterative procedure avoids being trapped within local
 290 minima. The overall algorithm applied here is as follows:

- 291 (1) Least squares cost function generation, the trace of the Gramian: $E_i = \text{Trace}\{(A -$
 292 $B) \times (A - B)^T\}$ where $A - B$ is a matrix of residuals, the difference be-
 293 tween simulated A and experimental absorption spectra B . If this is the
 294 initial step, a generalized temperature is defined $T \approx E_i$
- 295 (2) Each unconstrained parameter x is changed by a random amount $\pm\Delta x$,
 296 sampled from the uniform distribution $[0, 1)$. The corresponding energy
 297 E_f is calculated as before.
- 298 (3) If $E_f < E_i$, the change is accepted, else,
- 299 (4) Parameter changes are accepted or rejected in the traditional Metropo-
 300 liss [44] scheme, using the probabilistic factor: $e^{-(E_f - E_i)/T}$
- 301 (5) The process is repeated and the temperature lowered according to some
 302 schedule, until such time as convergence is reached.

303 In order to give confidence intervals for parameters

$$304 \quad \phi = \{\lambda_1^k, \lambda_2^k, \epsilon^k, \mu_x^k, \sigma_x^k, \mu_y^k, \sigma_y^k, \rho^k, \eta^k, \mathcal{A}^k; k = 1, \dots, L\}$$

305 optimized in the simulation, strictly speaking the measurement or MQMAS
 306 experiment in conjunction with simulations ought to be repeated and statistics
 307 created from fitted data. However, owing to the considerable time multiple ex-
 308 periments and simulations requires, a more suitable approach to error analysis
 309 is found in statistical re-sampling, such as jackknifing or bootstrapping [29].
 310 In the original jackknife approach, $\bar{\phi}_{-i}$ is defined as the least squared estimate
 311 of parameter ϕ when the i th data point of n total is removed from the set.
 312 Pseudo values are created,

$$313 \quad P_i = n\bar{\phi} - (n-1)\bar{\phi}_{-i} \quad (34)$$

314 with average \bar{P} and variance matrix V_P :

$$315 \quad \bar{P} = \bar{\phi}_J = n^{-1} \sum_{i=1}^n P_i \quad (35)$$

$$316 \quad nV_P = \frac{1}{n-1} \sum_{i=1}^n (P_i - \bar{P})(P_i - \bar{P})^T \quad (36)$$

317 In the present application, this method implies $n+1$ non-linear optimizations
 318 which is still far too time consuming. Fox et al [58] propose a solution in the
 319 form of an approximate jackknife, which requires instead a single non-linear
 320 optimization, via a Taylor expansion of the least squares estimate equation
 321 for $\bar{\phi}_i$, assuming it is a stationary point for the sum of the residuals. In this
 322 method, an estimate of the variance matrix is given by:

$$323 \quad V = (Z^T Z)^{-1} \sum_{j=1}^n z_j z_j^T r_j^2 (Z^T Z)^{-1} \quad (37)$$

324 where:

$$325 \quad z_i = \nabla f(x_i, \phi) = \left\{ \frac{\partial}{\partial \phi_1} f(x_i, \phi) \dots \frac{\partial}{\partial \phi_l} f(x_i, \phi) \right\}_{\phi=\bar{\phi}}^T \quad (38)$$

$$326 \quad Z^T = (z_1, \dots, z_n) \quad (39)$$

327 and r_i is the vector of residuals. The model as presented here consists of ten
 328 free parameters per chemical site (ie., $l=10$), so in the case of N chemical
 329 sites, this corresponds to the creation of a $10N \times 10N$ variance matrix from
 330 the quantities listed here. These are evaluated at best-fit parameters $\bar{\phi}$, using
 331 the partial derivatives as listed in Appendix B.

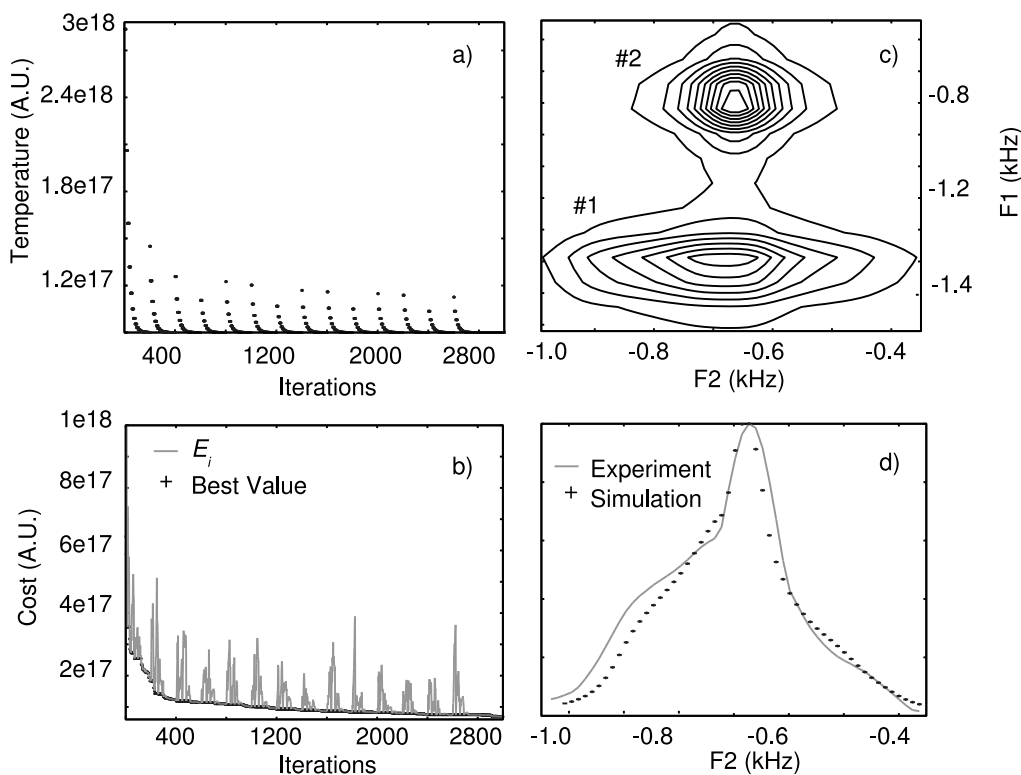


Fig. 5. (a) Annealing schedule versus iterations; temperature is rapidly annealed and reannealed (b) Variation of energy and best energy value versus iteration. In addition to the algorithm outlined, a separate heuristic is applied whereby every p steps, the parameter values are reset to their best values to date corresponding to the stored best energy value (c) Simulated MQMAS spectrum. Comparing with fig. 2b, while the general shape and peak positions have been re-produced, small differences arising from distributed values are apparent. The number of powder increments used was 1597 (d) Comparison of simulated and experimental F2 frequency projection

333 The aforementioned theory was implemented in C, using a number of func-
 334 tions from the GNU Scientific Library (GSL), as well as the math and stan-
 335 dard libraries. A single application was written which performs calculations
 336 of frequency equation 29 as a function of each powder angle α, β according
 337 to the ZCW scheme. For each frequency dimension Sobol sequences are gen-
 338 erated and used to create bi-variate distributions of isotropic chemical shift
 339 and quadrupole coupling constant according to the given algorithm. Finally,
 340 summation over powder angles and variates are performed using the kernel of
 341 eq. 30. The results of initial simulations pointed to single values of asymme-
 342 try parameter being sufficient for distinct chemical sites. A single OpenMP
 343 pragma was used to parallelize inner frequency loops,

344 `#pragma omp parallel for private(h,i)`

345 using the private declaration on loop indices to prevent a race condition oc-
 346 ccurring between separate threads. The OpenMP application programming in-
 347 terface is essentially a set of libraries and associated compiler directives which
 348 permits shared memory processing (SMP) on machines with the appropri-
 349 ate hardware. In order to perform optimization of the simulation parameters,
 350 the simulated annealing algorithm was implemented in the OCTAVE script-
 351 ing language. This allowed for tuning of heuristic parameters, particularly the
 352 annealing schedule and size of random fluctuations taken by individual param-
 353 eters per iteration. In addition, parameter values corresponding to the lowest
 354 energy obtained are stored every iteration and used for occasional resets. In
 355 order to determine the appropriate number of crystallite orientations neces-
 356 sary for a simulation as well as sample numbers from the distribution, the
 357 MQMAS spectrum of the tetrahedral region within simple-crystalline model
 358 compound VPI-5 was simulated and results are displayed in figure 5.

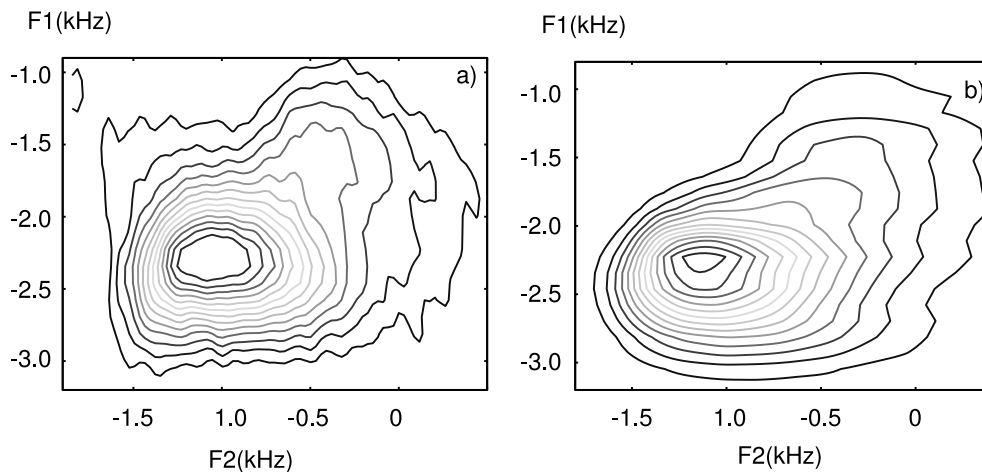


Fig. 6. (a) ^{27}Al 3QMAS experimental spectrum, hydrous aluminosilicate. Thir-
 teen equally spaced contours are drawn from 10 to 90% of the total intensity
 (b)Simulation for the same

359 It is anticipated that the number of crystallite orientations required for ad-
 360 equate convergence in a particular summation will increase with linewidth,
 361 which in turn is proportional to the quadrupole coupling constant. Fitting to
 362 a crystalline model compound provides a good means of determining the min-
 363 imum number of crystallite orientations required for a comparable linewidth.

Table 2

Results for simulation of hydrous aluminosilicate MQMAS spectrum

Site #	$\delta_{iso}^{cs} (Hz)$		$C_q (MHz)$		η	Area
	μ	σ	μ	σ		
1	-1399	127	2.9	0.9	0.52	0.39
2	-1163	333	3.3	0.8	0.52	0.49
3	-747	167	3.6	1.7	0.23	0.12

Table 3

Jackknife parameter error estimates for simulation of hydrous aluminosilicate MQMAS spectrum

Site #	$\delta_{iso}^{cs} (%)$		$C_q (%)$		$\eta (%)$	Area (%)
	μ	σ	μ	σ		
1	0.5	5.1	3.8	4.5	0.7	12.2
2	2.1	4.9	4.7	6.6	1.1	21.1
3	2.9	8.6	15.7	14.8	7.2	31

364 Convergence or lack thereof is more easily observed in a crystalline system as
365 compared to a more disordered material, which is devoid of the characteristic
366 features. In this case, 1597 angle pairs (F_{17}) were minimal for quadrupole cou-
367 pling constants in the range less than 4MHz, as determined from ^{27}Al (spin
368 $I = 5/2$) MQMAS of VPI-5. The Second Order Quadrupole Effect (SOQE) pa-
369 rameters³ determined from the simulation for the tetrahedral region of VPI-5
370 were 2.6 and 1.15 MHz, which compare favorably with literature values [10].

371 Using the same number of crystallite angles, optimized simulations were per-
372 formed for the tetrahedral region within a hydrated aluminosilicate sample,
373 using 200 samples for each of three bi-variate distributions and results are
374 displayed in figure 6 and table 2. The Gaussian/Lorentzian ratio, correlation
375 coefficient and broadening constants in both dimensions were constrained to
376 0.5, 0, and 100 Hz respectively and 1000 simulated annealing iterations were
377 performed. The experimental spectra displays regions of both order (narrow,
378 horizontal peaks) and disorder (broad, indistinct). In order to test the validity
379 of the simulated, optimized model, jackknife parameter error estimates were
380 determined and are presented in table 3.

381

382

³ SOQE = $C_q \sqrt{1 + \frac{\eta^2}{3}}$

383 The chemical sites with narrow distributions (assigned here to crystalline al-
384 bite and zeolitic material) have corresponding parameters with least error. This
385 may be attributed to a number of factors, in this case most likely to the lower
386 signal to noise ratio of the disordered region, assigned here to amorphous albite
387 glass. For chemical sites with larger quadrupole coupling constants, there is
388 also the possibility that due to experimental excitation deficiency, the second
389 order perturbation frequency expression breaks down. Finally, the assump-
390 tions of a Gaussian statistical model may be inappropriate for the system
391 in question. As mentioned earlier, model distributions reflect the underlying
392 stochastic nature of bonding in a disordered material. Regardless of the con-
393 vention applied in describing the EFG tensor, the sign on the quadrupole
394 coupling constant should be single valued and therefore a more appropriate
395 distribution may be found in the positive tailed log-normal distribution. Under
396 this assumption, random variable y representing the quadrupole coupling con-
397 stant is transformed as $z = \exp(y)$, *ie.*, $y = \log(z)$. The resulting distribution
398 would be a bi-variate normal-lognormal distribution in the chemical shielding
399 and quadrupole coupling constant respectively.

400 4 Conclusions

401 Theory has been outlined and an application implemented in the C program-
402 ming language that permits the simulation of an MQMAS spectrum, as a func-
403 tion of underlying parameter distributions. This simulation relies on the use of
404 quasi-Monte Carlo variates to promote convergence and utilizes the OpenMP
405 library to permit execution on SMP machines. Owing to the manner in which
406 random variates are created in the application, the program is amenable to
407 High Throughput Computing (HTC) platforms such as Condor or PBS. Dif-
408 ferent nodes within a cluster or grid can be attributed different sections of
409 the sample space using a submission script. In addition, an OCTAVE script
410 implementing a simulated annealing algorithm is used to optimize the simu-
411 lation, providing reliable estimates of NMR parameters. Finally, theory was
412 outlined and implemented for providing parameter variance estimates using a
413 jackknife approach. As an alternative to the essentially parametric approach
414 outlined here, the application may be used to optimize a very large number
415 of chemical sites of equal amplitude. In this event, kernel density estimation
416 may be applied to parameter estimates to provide a more arbitrary probabil-
417 ity distribution model for chemical order. In conjunction with the MQMAS
418 experiment, the application described herein enables the characterization of
419 materials which may vary greatly in the degree of underlying chemical and
420 structural order.

421 **Acknowledgements**

422 Jeff Nucciarone and the Research Computing and Cyberinfrastructure group
 423 at Penn State are acknowledged for their generous assistance and use of com-
 424 putational resources. Marek Pruski kindly provided the MQMAS spinsight
 425 pulse sequence used for experiments. This work has been funded via National
 426 Science Foundation grant number CHE 0535656

427 **Appendix A**

428
$$P_2(\theta) = \frac{1}{2} (3 \cos^2 \theta - 1)$$

429
$$P_4(\theta) = \frac{1}{8} (35 \cos^4 \theta - 30 \cos^2 \theta + 3)$$

430
$$V_{2,0} = \frac{1}{2} \sqrt{6} V_{zz}; V_{2,1} = -V_{xz} - iV_{yz}$$

431
$$V_{2,-1} = V_{xz} - iV_{yz}; V_{2,2} = \frac{1}{2} (V_{xx} - V_{yy}) + iV_{xy}$$

432
$$V_{2,-2} = \frac{1}{2} (V_{xx} - V_{yy}) - iV_{xy}; K^{(2,0)} = \frac{1}{\sqrt{6}} [3I_z^2 - I(I+1)]$$

433
$$K^{(2,1)} = -\frac{1}{2} I_+ (2I_z + 1); K^{(2,-1)} = \frac{1}{2} I_- (2I_z - 1)$$

434
$$K^{(2,2)} = \frac{1}{2} I_- I_-$$

435
$$A^{(4)}(I, r, c) = 18I(I+1) - 34(r^2 + rc + c^2) - 5$$

436
$$A^{(2)}(I, r, c) = 8I(I+1) - 12(r^2 + rc + c^2) - 3$$

437
$$A^{(0)}(I, r, c) = I(I+1) - 3(r^2 + rc + c^2)$$

438 **Appendix B**

439 Referring to equation 31, the kernal of the integrand is:

440
$$\mathcal{I} =$$

$$\left(\frac{e^{-\frac{(f_2-f_{2m})^2}{2\lambda_2^2} - \frac{(f_1-f_{1m})^2}{2\lambda_1^2}} \epsilon + \frac{\lambda_1 \lambda_2 (1-\epsilon)}{(\lambda_1^2 + (f_1-f_{1m})^2)(\lambda_2^2 + (f_2-f_{2m})^2)}}{2\pi \lambda_1 \lambda_2} \right) e^{-\frac{\frac{(y-\mu_y)^2}{\sigma_y^2} - \frac{2\rho(x-\mu_x)(y-\mu_y)}{\sigma_x \sigma_y} + \frac{(x-\mu_x)^2}{\sigma_x^2}}{2(1-\rho^2)}} \mathcal{A}$$

441 $2\pi \sqrt{1-\rho^2} \sigma_x \sigma_y$

442 where it is understood that the total intensity is computed via summation of \mathcal{I}
443 over all L chemical sites, as well as powder angles α, β . Each partial derivative
444 listed is performed independently for each chemical site and the total variance
445 matrix calculated in the manner described previously. Random variates for
446 chemical shift and quadrupole coupling constant are x and y respectively, with
447 corresponding mean μ and standard deviation σ labeled with the appropriate
448 subscript. Frequency coefficients:

449 $clb_0 = -I(I+1) + 3/4$

450 $clb_1 = -18I(I+1) + 34/4 + 5$

451 $clb_2 = (r-c)(I(I+1) - 3(r^2 + rc + c^2))$

452 $clb_3 = (r-c)(18I(I+1) - 34(r^2 + rc + c^2) - 5)$

453 Derivatives:

454 $\frac{\partial \mathcal{I}}{\partial \eta} = \frac{\partial \mathcal{I}}{\partial f_{1m}} \frac{df_{1m}}{d\eta} + \frac{\partial \mathcal{I}}{\partial f_{2m}} \frac{df_{2m}}{d\eta}$

455 $\frac{df_{2m}}{d\eta} =$

456 $\frac{clb_1 y^2}{11520 f_0 I^2 (2I-1)^2} \left\{ \cos^2 \beta (140 \cos(4.0\alpha)\eta + 60.0\eta - 480 \cos(2\alpha)) + \right.$

457 $\left. \cos^4 \beta (-70.0 \cos(4\alpha)\eta - 70.0\eta + 420 \cos(2\alpha)) - 70.0 \cos(4.0\alpha)\eta - 6.0\eta + 60.0 \cos(2\alpha) \right\}$

458 $-\frac{clb_0 y^2 \eta}{5 f_0 I^2 (2I-1)^2}$

459 $\frac{df_{1m}}{d\eta} =$

460 $\frac{-k \cdot clb_1 y^2}{11520 f_0 I^2 (2I-1)^2} \left\{ \cos^2 \beta (140 \cos(4.0\alpha)\eta + 60.0\eta - 480 \cos(2\alpha)) + \right.$

461 $\left. \cos^4 \beta (-70.0 \cos(4\alpha)\eta - 70.0\eta + 420 \cos(2\alpha)) - 70.0 \cos(4.0\alpha)\eta - 6.0\eta + 60.0 \cos(2\alpha) \right\}$

$$\begin{aligned}
& + \frac{k \cdot clb_0 y^2 \eta}{5 f_0 I^2 (2I - 1)^2} - \frac{clb_2 y^2}{11520 f_0 I^2 (2I - 1)^2} \left\{ \cos^2 \beta (140 \cos(4.0\alpha) \eta + 60.0\eta - 480 \cos(2\alpha)) + \right. \\
& \cos^4 \beta (-70.0 \cos(4\alpha) \eta - 70.0\eta + 420 \cos(2\alpha)) - 70.0 \cos(4.0\alpha) \eta - 6.0\eta + 60.0 \cos(2\alpha) \left. \right\} \\
& + \frac{clb_3 y^2 \eta}{5 f_0 I^2 (2I - 1)^2}
\end{aligned}$$

where k is the shear factor.

$$\frac{\partial \mathcal{I}}{\partial f 2_m} =$$

$$\frac{\left(\frac{(f2-f2_m) e^{-\frac{(f2-f2_m)^2}{2\lambda_2^2} - \frac{(f1-f1_m)^2}{2\lambda_1^2}} \epsilon + \frac{2(f2-f2_m)\lambda_1\lambda_2(1-\epsilon)}{(\lambda_1^2+(f1-f1_m)^2)(\lambda_2^2+(f2-f2_m)^2)^2}}{2\pi\lambda_1\lambda_2^3} \right) e^{-\frac{\frac{(y-\mu_y)^2}{\sigma_y^2} - \frac{2\rho(x-\mu_x)(y-\mu_y)}{\sigma_x\sigma_y} + \frac{(x-\mu_x)^2}{\sigma_x^2}}{2(1-\rho^2)}}}{2\pi\sqrt{1-\rho^2}\sigma_x\sigma_y} \mathcal{A}$$

$$\frac{\partial \mathcal{I}}{\partial f 1_m} =$$

$$\frac{\left(\frac{(f1-f1_m) e^{-\frac{(f1-f1_m)^2}{2\lambda_1^2} - \frac{(f2-f2_m)^2}{2\lambda_2^2}} \epsilon + \frac{2(f1-f1_m)\lambda_2\lambda_1(1-\epsilon)}{(\lambda_2^2+(f2-f2_m)^2)(\lambda_1^2+(f1-f1_m)^2)^2}}{2\pi\lambda_2\lambda_1^3} \right) e^{-\frac{\frac{(y-\mu_y)^2}{\sigma_y^2} - \frac{2\rho(x-\mu_x)(y-\mu_y)}{\sigma_x\sigma_y} + \frac{(x-\mu_x)^2}{\sigma_x^2}}{2(1-\rho^2)}}}{2\pi\sqrt{1-\rho^2}\sigma_x\sigma_y} \mathcal{A}$$

$$\frac{\partial \mathcal{I}}{\partial \lambda_2} =$$

$$\frac{\mathcal{A}}{2\pi\sqrt{1-\rho^2}\sigma_x\sigma_y} \left(-\frac{e^{-\frac{(f2-f2_m)^2}{2\lambda_2^2} - \frac{(f1-f1_m)^2}{2\lambda_1^2}} \epsilon}{2\pi\lambda_1\lambda_2^2} + \frac{(f2-f2_m)^2 e^{-\frac{(f2-f2_m)^2}{2\lambda_2^2} - \frac{(f1-f1_m)^2}{2\lambda_1^2}} \epsilon}{2\pi\lambda_1\lambda_2^4} + \right. \\
\left. \frac{\lambda_1(1-\epsilon)}{(\lambda_1^2+(f1-f1_m)^2)(\lambda_2^2+(f2-f2_m)^2)} - \frac{2\lambda_1\lambda_2^2(1-\epsilon)}{(\lambda_1^2+(f1-f1_m)^2)(\lambda_2^2+(f2-f2_m)^2)^2} \right) \times \\
e^{-\frac{\frac{(y-\mu_y)^2}{\sigma_y^2} - \frac{2\rho(x-\mu_x)(y-\mu_y)}{\sigma_x\sigma_y} + \frac{(x-\mu_x)^2}{\sigma_x^2}}{2(1-\rho^2)}}$$

$$\frac{\partial \mathcal{I}}{\partial \lambda_1} =$$

$$\frac{\mathcal{A}}{2 \pi \sqrt{1 - \rho^2} \sigma_x \sigma_y} \left(- \frac{e^{-\frac{(f_2 - f_{2m})^2}{2 \lambda_2^2} - \frac{(f_1 - f_{1m})^2}{2 \lambda_1^2}} \epsilon}{2 \pi \lambda_1^2 \lambda_2} + \frac{(f_1 - f_{1m})^2 e^{-\frac{(f_2 - f_{2m})^2}{2 \lambda_2^2} - \frac{(f_1 - f_{1m})^2}{2 \lambda_1^2}} \epsilon}{2 \pi \lambda_1^4 \lambda_2} + \right. \\ \left. \frac{\lambda_2 (1 - \epsilon)}{(\lambda_1^2 + (f_1 - f_{1m})^2) (\lambda_2^2 + (f_2 - f_{2m})^2)} - \frac{2 \lambda_1^2 \lambda_2 (1 - \epsilon)}{(\lambda_1^2 + (f_1 - f_{1m})^2)^2 (\lambda_2^2 + (f_2 - f_{2m})^2)} \right) \times \\ e^{-\frac{\frac{(y - \mu_y)^2}{\sigma_y^2} - \frac{2 \rho (x - \mu_x)(y - \mu_y)}{\sigma_x \sigma_y} + \frac{(x - \mu_x)^2}{\sigma_x^2}}{2(1 - \rho^2)}}$$

$$\frac{\partial \mathcal{I}}{\partial \rho} =$$

$$\left(\frac{e^{-\frac{(f_2 - f_{2m})^2}{2 \lambda_2^2} - \frac{(f_1 - f_{1m})^2}{2 \lambda_1^2}} \epsilon}{2 \pi \lambda_1 \lambda_2} + \frac{\lambda_1 \lambda_2 (1 - \epsilon)}{(\lambda_1^2 + (f_1 - f_{1m})^2) (\lambda_2^2 + (f_2 - f_{2m})^2)} \right) e^{-\frac{\frac{(y - \mu_y)^2}{\sigma_y^2} - \frac{2 \rho (x - \mu_x)(y - \mu_y)}{\sigma_x \sigma_y} + \frac{(x - \mu_x)^2}{\sigma_x^2}}{2(1 - \rho^2)}} \mathcal{A} \\ \frac{2 \pi \sqrt{1 - \rho^2} \sigma_x \sigma_y}{471}$$

$$\times \left(\frac{\rho}{(1 - \rho^2)} - \frac{\rho (x - \mu_x)^2}{(1 - \rho^2)^2 \sigma_x} + \frac{(x - \mu_x)(y - \mu_y)}{(1 - \rho^2) \sigma_x \sigma_y} + \frac{2 \rho^2 (x - \mu_x)}{(1 - \rho^2) \sigma_x \sigma_y} - \frac{\rho (y - \mu_y)^2}{(1 - \rho^2)^2 \sigma_y} \right) \\ 472$$

$$\frac{\partial \mathcal{I}}{\partial \sigma_y} =$$

$$- \frac{\mathcal{A}}{4 \pi (1 - \rho^2)^{\frac{3}{2}} \sigma_x \sigma_y} \left(\frac{e^{-\frac{(f_2 - f_{2m})^2}{2 \lambda_2^2} - \frac{(f_1 - f_{1m})^2}{2 \lambda_1^2}} \epsilon}{2 \pi \lambda_1 \lambda_2} + \frac{\lambda_1 \lambda_2 (1 - \epsilon)}{(\lambda_1^2 + (f_1 - f_{1m})^2) (\lambda_2^2 + (f_2 - f_{2m})^2)} \right) \times \\ \left(\frac{2 \rho (x - \mu_x)(y - \mu_y)}{\sigma_x \sigma_y^2} - \frac{2 (y - \mu_y)^2}{\sigma_y^3} \right) e^{-\frac{\frac{(y - \mu_y)^2}{\sigma_y^2} - \frac{2 \rho (x - \mu_x)(y - \mu_y)}{\sigma_x \sigma_y} + \frac{(x - \mu_x)^2}{\sigma_x^2}}{2(1 - \rho^2)}} \\ \frac{2 \pi \sqrt{1 - \rho^2} \sigma_x \sigma_y^2}{473} \\ \left(\frac{e^{-\frac{(f_2 - f_{2m})^2}{2 \lambda_2^2} - \frac{(f_1 - f_{1m})^2}{2 \lambda_1^2}} \epsilon}{2 \pi \lambda_1 \lambda_2} + \frac{\lambda_1 \lambda_2 (1 - \epsilon)}{(\lambda_1^2 + (f_1 - f_{1m})^2) (\lambda_2^2 + (f_2 - f_{2m})^2)} \right) e^{-\frac{\frac{(y - \mu_y)^2}{\sigma_y^2} - \frac{2 \rho (x - \mu_x)(y - \mu_y)}{\sigma_x \sigma_y} + \frac{(x - \mu_x)^2}{\sigma_x^2}}{2(1 - \rho^2)}} \mathcal{A} \\ \frac{2 \pi \sqrt{1 - \rho^2} \sigma_x \sigma_y^2}{473}$$

$$\frac{\partial \mathcal{I}}{\partial \mu_y} =$$

$$-\left(\frac{e^{-\frac{(f2-f2m)^2}{2\lambda_2^2} - \frac{(f1-f1m)^2}{2\lambda_1^2}} \epsilon}{2\pi \lambda_1 \lambda_2} + \frac{\lambda_1 \lambda_2 (1-\epsilon)}{(\lambda_1^2 + (f1-f1m)^2)(\lambda_2^2 + (f2-f2m)^2)} \right) \times$$

$$\frac{\left(\frac{2\rho(x-\mu_x)}{\sigma_x \sigma_y} - \frac{2(y-\mu_y)}{\sigma_y^2} \right) e^{-\frac{\frac{(y-\mu_y)^2}{\sigma_y^2} - \frac{2\rho(x-\mu_x)(y-\mu_y)}{\sigma_x \sigma_y} + \frac{(x-\mu_x)^2}{\sigma_x^2}}{2(1-\rho^2)}} \mathcal{A}}{4\pi (1-\rho^2)^{\frac{3}{2}} \sigma_x \sigma_y}$$

$$\frac{\partial \mathcal{I}}{\partial \sigma_x} =$$

$$-\frac{\mathcal{A}}{4\pi (1-\rho^2)^{\frac{3}{2}} \sigma_y \sigma_x} \left(\frac{e^{-\frac{(f2-f2m)^2}{2\lambda_2^2} - \frac{(f1-f1m)^2}{2\lambda_1^2}} \epsilon}{2\pi \lambda_1 \lambda_2} + \frac{\lambda_1 \lambda_2 (1-\epsilon)}{(\lambda_1^2 + (f1-f1m)^2)(\lambda_2^2 + (f2-f2m)^2)} \right) \times$$

$$\left(\frac{2\rho(y-\mu_y)(x-\mu_x)}{\sigma_y \sigma_x^2} - \frac{2(x-\mu_x)^2}{\sigma_x^3} \right) e^{-\frac{\frac{(x-\mu_x)^2}{\sigma_x^2} - \frac{2\rho(y-\mu_y)(x-\mu_x)}{\sigma_y \sigma_x} + \frac{(y-\mu_y)^2}{\sigma_y^2}}{2(1-\rho^2)}}$$

$$-\frac{\left(\frac{e^{-\frac{(f2-f2m)^2}{2\lambda_2^2} - \frac{(f1-f1m)^2}{2\lambda_1^2}} \epsilon}{2\pi \lambda_1 \lambda_2} + \frac{\lambda_1 \lambda_2 (1-\epsilon)}{(\lambda_1^2 + (f1-f1m)^2)(\lambda_2^2 + (f2-f2m)^2)} \right) e^{-\frac{\frac{(x-\mu_x)^2}{\sigma_x^2} - \frac{2\rho(y-\mu_y)(x-\mu_x)}{\sigma_y \sigma_x} + \frac{(y-\mu_y)^2}{\sigma_y^2}}{2(1-\rho^2)}} \mathcal{A}}{2\pi \sqrt{1-\rho^2} \sigma_y \sigma_x^2}$$

$$\frac{\partial \mathcal{I}}{\partial \mu_x} =$$

$$-\left(\frac{e^{-\frac{(f2-f2m)^2}{2\lambda_2^2} - \frac{(f1-f1m)^2}{2\lambda_1^2}} \epsilon}{2\pi \lambda_1 \lambda_2} + \frac{\lambda_1 \lambda_2 (1-\epsilon)}{(\lambda_1^2 + (f1-f1m)^2)(\lambda_2^2 + (f2-f2m)^2)} \right) \times$$

$$\frac{\left(\frac{2\rho(y-\mu_y)}{\sigma_y \sigma_x} - \frac{2(x-\mu_x)}{\sigma_x^2} \right) e^{-\frac{\frac{(x-\mu_x)^2}{\sigma_x^2} - \frac{2\rho(y-\mu_y)(x-\mu_x)}{\sigma_y \sigma_x} + \frac{(y-\mu_y)^2}{\sigma_y^2}}{2(1-\rho^2)}} \mathcal{A}}{4\pi (1-\rho^2)^{\frac{3}{2}} \sigma_y \sigma_x}$$

477 $\frac{\partial \mathcal{I}}{\partial \mathcal{A}} =$

$$\frac{\left(e^{-\frac{(f_2-f_{2m})^2}{2\lambda_2^2} - \frac{(f_1-f_{1m})^2}{2\lambda_1^2}} \epsilon + \frac{\lambda_1 \lambda_2 (1-\epsilon)}{(\lambda_1^2 + (f_1-f_{1m})^2)(\lambda_2^2 + (f_2-f_{2m})^2)} \right) e^{-\frac{(y-\mu_y)^2}{\sigma_y^2} - \frac{2\rho(x-\mu_x)(y-\mu_y)}{\sigma_x \sigma_y} + \frac{(x-\mu_x)^2}{\sigma_x^2}}}{2\pi \sqrt{1-\rho^2} \sigma_x \sigma_y}$$

478

479 **References**

- 480 [1] R. S. Dumont A. D. Bain. Introduction to Floquet theory: The calculation
 481 of spinning sideband intensities in magic-angle spinning NMR. *Concepts in*
 482 *Magnetic Resonance*, 13:159–170, 2001.
- 483 [2] A. Medek, J. S. Harwood, L. Frydman. Multiple-quantum MAS NMR: a new
 484 method for the study of quadrupolar nuclei in solids. *Journal of the American*
 485 *Chemical Society*, 117:12779–12787, 1995.
- 486 [3] R. Verhagen A. P. M. Kentgens. Quantitative excitation of half-integer
 487 quadrupolar nuclei by a frequency-stepped adiabatic half-passage. *Journal of*
 488 *Magnetic Resonance*, 95:619–625, 1991.
- 489 [4] R. Verhagen A. P. M. Kentgens. Advantages of double frequency sweeps in
 490 static, MAS and MQMAS NMR of spin $I = 3/2$ nuclei. *Chemical Physics*
 491 *Letters*, 300:435–443, 1999.
- 492 [5] A. Pines A. Samoson, E. Lippmaa. High resolution solid-state nmr. averaging
 493 of second-order effects by means of a double-rotor. *Molecular Physics*, 65:1013–
 494 1018, 1988.
- 495 [6] E. Lippmaa A. Samoson. 2d nutation spectroscopy in solids. *Journal of*
 496 *Magnetic Resonance*, 79:255–268, 1988.
- 497 [7] S. Vega A. Schmidt. The floquet theory of magnetic resonance spectroscopy
 498 of single spins and dipolar coupled spin-pairs in rotating solids. *Journal of*
 499 *Chemical Physics*, 96:2655–2680, 1992.
- 500 [8] A. Abragam. *The Principles of Nuclear Magnetism*. Oxford: Clarendon Press,
 501 1962.
- 502 [9] B. Bureau, G. Silly, J. Y. Buzare, C. Legein, D. Massiot. From crystalline to
 503 glassy gallium fluoride materials: an NMR study of ^{69}Ga and ^{71}Ga quadrupolar
 504 nuclei. *Solid State Nuclear Magnetic Resonance*, 15:129–138, 1999.
- 505 [10] J. Rocha M. Pruski C. Fernandez, C. Morais. High-Resolution Heteronuclear
 506 Correlation Spectra between ^{31}P and ^{27}Al in Microporous Aluminophosphates.
 507 *Solid State Nuclear Magnetic Resonance*, 21:61–70, 2002.

- 508 [11] P. A. Casabella. Determination of nuclear quadrupole coupling constants from
509 nuclear magnetic resonance in polycrystalline solids. *Journal of Chemical*
510 *Physics*, 40:149–152, 1964.
- 511 [12] H. Conroy. Molecular Schrodinger Equation VIII. A new method for the
512 evaluation of multidimensional integrals. *Journal of Chemical Physics*, 47:5307–
513 5318, 1967.
- 514 [13] Z. Zimpel D. F. Howarth, J. A. Weil. Generalization of the lineshape useful in
515 magnetic resonance spectroscopy. *Journal of Magnetic Resonance*, 161:215–221,
516 2003.
- 517 [14] D. Trumeau J. P. Coutures J. Virlet-P. Florian P. J. Grandinetti D. Massiot,
518 B. Touzo. Two-dimensional magic-angle spinning isotropic reconstruction
519 sequences for quadrupolar nuclei. *Solid State Nuclear Magnetic Resonance*,
520 6:73–83, 1996.
- 521 [15] M. Capron I. King S. Le Calve-B. Alonso J-O. Durand B. Bujoli Z. Gan
522 G. Hoatson D. Massiot, F. Fayon. Modelling one- and two-dimensional solid-
523 state NMR spectra. *Magnetic Resonance in Chemistry*, 40:70–76, 2002.
- 524 [16] D. M. Grant D. W. Alderman, M. S. Solum. Methods for analyzing
525 spectroscopic lineshapes. NMR solid powder patterns. *Journal of Chemical*
526 *Physics*, 84:3717–3725, 1986.
- 527 [17] D.J. States, R. A. Haberkorn, D. J. Ruben. A Two-Dimensional Nuclear
528 Overhauser Experiment with Pure Absorption Phase in Four Quadrants.
529 *Journal of Magnetic Resonance*, 48:286–292, 1982.
- 530 [18] R. G. Eades E. R. Andrew, A. Bradbury. Removal of dipolar broadening of
531 nuclear magnetic resonance spectra of solids by specimen rotation. *Nature*,
532 183:1802–1803, 1959.
- 533 [19] F. Angeli, T. Charpentier, P. Faucon, J-C. Petit. Structural Characterization
534 of Glass from the Inversion of ^{23}Na and ^{27}Al 3Q-MAS NMR Spectra. *Journal*
535 *of Physical Chemistry B*, 103:10356–10364, 1999.
- 536 [20] I. H. Sloan F. Y. Kuo. Quasi-monte carlo methods can be efficient for integration
537 over products of spheres. *Journal of Complexity*, 21:196–210, 2005.
- 538 [21] W. Freedon. On integral formulas of the (unit) sphere and their application to
539 numerical computation of integrals. *Computing*, 25:131–146, 1980.
- 540 [22] G. Czjek, J. Fink, F. Gotz, H. Schmidt, J. M. D. Coey, J-P. Rebouillat, A.
541 Lienard. Atomic coordination and the distribution of electric field gradients in
542 amorphous solids. *Physical Review B*, 23:2513–2530, 1981.
- 543 [23] G. L. Hoaston, D. H. Zhou, F. Fayon, D. Massiot, R. L. Vold. ^{93}Nb
544 magic angle spinning NMR study of perovskite relaxor ferroelectrics $(1-$
545 $x)\text{Pb}(\text{Mg}_{1/3}\text{Nb}_{2/3})\text{O}_3-x\text{Pb}(\text{Sc}_{1/2}\text{Nb}_{1/2})\text{O}_3$. *Physical Review B*, 66:224103(13),
546 2002.

- 547 [24] Z. Gan. Double-quantum filtered stmas. *Journal of Magnetic Resonance*,
548 164:369–372, 2003.
- 549 [25] Z. H. Gan. Isotropic NMR Spectra of Half-Integer Quadrupolar Nuclei Using
550 Satellite Transitions and Magic-Angle Spinning. *Journal of the American*
551 *Chemical Society*, 122:3242–3243, 2000.
- 552 [26] I. Farnan J. H. Kristensen. Efficient solid state NMR powder simulations using
553 SMP and MPP parallel computation. *Journal of Magnetic Resonance*, 161:183–
554 190, 2003.
- 555 [27] R. L. Vold J. H. Kristensen, G. L. Hoatson. Design and Implementation of
556 Runge-Kutta Methods for MAS NMR Lineshapes. *Journal of Computational*
557 *Physics*, 170:415–447, 2001.
- 558 [28] S. Steuernagel J-P. Amoureux, C. Fernandez. Z Filtering in MQMAS NMR.
559 *Journal of Magnetic Resonance, Series A*, 123:116–118, 1996.
- 560 [29] D. Tu J. Shao. *The Jackknife and Bootstrap*. Springer-Verlag, 1995.
- 561 [30] J. Skibsted, N. Nielson, H. Bildsoe, H. J. Jakobsen. Satellite Transitions in
562 MAS NMR Spectra of Quadrupolar Nuclei. *Journal of Magnetic Resonance*,
563 95:88–117, 1991.
- 564 [31] S. Kirkpatrick, C. D. Gelatt, and M. P. Vecchi. Optimization by simulated
565 annealing. *Science*, 220(4598):671–680, 1983.
- 566 [32] A. Pines K.T. Mueller, E. W. Wooten. Dynamic Angle Spinning of Quadrupolar
567 Nuclei. *Journal of Magnetic Resonance*, 92:620–, 1991.
- 568 [33] G. C. Chingas J. W. Zwanziger K.T. Mueller, B. Q. Sun. Dynamic Angle
569 Spinning of Quadrupolar Nuclei. *Journal of Magnetic Resonance*, 86:470–487,
570 1990.
- 571 [34] R. Kubo. A general theory of magnetic resonance absorption. *Journal of the*
572 *Physical Society of Japan*, 9:888–, 1954.
- 573 [35] M. Bak, J. T. Rasmussen, N. C. Nielsen. SIMPSON: A General Simulation
574 Program for Solid-State NMR Spectroscopy. *Journal of Magnetic Resonance*,
575 147:296–330, 2000.
- 576 [36] F. Rief M. H. Cohen. *Solid State Physics*. Academic, 1957.
- 577 [37] J. S. Waugh M. Maricq. NMR in rotating solids. *Journal of Physical Chemistry*,
578 70:3300–3316, 1979.
- 579 [38] W. Magnus. On the exponential solution of differential equations for a linear
580 operator. 7:649–673, 1954.
- 581 [39] P. P. Man. Second-order quadrupole effects on hahn echoes in fast-rotating
582 solids at the magic angle. *Physical Review B*, 55:8406–8424, 1997.

- 583 [40] P. P. Man. Scaling and labeling the high-resolution isotropic axis of two-
584 dimensional multiple-quantum magic-angle-spinning spectra of half-integer
585 quadrupole spins. *Physical Review B*, 58:2764–2782, 1998.
- 586 [41] M. Mehring. *Principles of High Resolution NMR in Solids*. Springer-Verlag,
587 1983.
- 588 [42] William J. Morokoff and Russel E. Caffisch. Quasi-random sequences and their
589 discrepancies. *SIAM J. Sci. Comput.*, 15(6):1251–1279, 1994.
- 590 [43] A-A. Quoineaud J. Rocha F. Thibault-Starzyk C. Fernandez N. Malicki,
591 L. Mafra. Multiplex MQMAS NMR of quadrupolar nuclei. *Solid State Nuclear*
592 *Magnetic Resonance*, 28:13–21, 2005.
- 593 [44] M. N. Rosenbluth A. H. Teller-E. Teller N. Metropolis, A. W. Rosenbluth.
594 Equation of state calculations by fast computing machines. *The Journal of*
595 *Chemical Physics*, 21:1087–1092, 1953.
- 596 [45] H. Niederreiter. *Random number generation and quasi-Monte Carlo methods*.
597 SIAM, 1992.
- 598 [46] L. Emsley P. Hodgkinson. Numerical simulation of solid-state NMR
599 experiments. *Progress in Nuclear Magnetic Resonance Spectroscopy*, 36:201–
600 239, 2000.
- 601 [47] L. Frydman S. Vega P. K. Madhu, A. Goldbourt. Sensitivity enhancement of
602 the MQMAS NMR experiment by fast amplitude modulation of the pulses.
603 *Chemical Physics Letters*, 307:41–47, 1999.
- 604 [48] M. H. Levitt P. K. Madhu. Signal enhancement in the triple-quantum magic-
605 angle spinning NMR of spins-3/2 in solids: the FAM-RIACT-FAM sequence.
606 *Journal of Magnetic Resonance*, 155:150–155, 2002.
- 607 [49] P. R. Bodart. Distributions of the Quadrupolar and Isotropic Chemical
608 Shift Interactions in Two-Dimensional Multiple-Quantum MAS NMR Spectra.
609 *Journal of Magnetic Resonance*, 133:207–209, 1998.
- 610 [50] A. Ponti. Simulation of magnetic resonance static powder lineshapes: a
611 quantitative assessment of spherical codes. *Journal of Magnetic Resonance*,
612 138:288–297, 1999.
- 613 [51] W. A. Anderson R. R. Ernst. Application of fourier transform spectroscopy to
614 magnetic resonance. *Review of Scientific Instruments*, 37:93–102, 1966.
- 615 [52] R. V. Pound. Nuclear Electric Quadrupole Interactions in Crystals. *Physical*
616 *Review*, 79:685–702, 1950.
- 617 [53] M. E. Rose. *Elementary theory of angular momentum*. J. Wiley and Sons, 1963.
- 618 [54] S. A. Smith, T. O. Levante, B. H. Meier, R. R. Ernst. Computer Simulations
619 in Magnetic Resonance. An Object Oriented Programming Approach. *Journal*
620 *of Magnetic Resonance*, 106a:75–105, 1994.

- 621 [55] C. A. McDowell S. Ding. Application of floquet theory to quadrupolar nuclear
622 spin- $\frac{5}{2}$ nuclei in solids undergoing sample rotation. *Molecular Physics*, 95:841–
623 848, 1998.
- 624 [56] J. P. Amoureux J. Cho S. W. Martin M. Pruski S.-J. Hwang, C. Fernandez.
625 Quantitative study of the short range order in B_2O_3 and B_2S_3 by MAS and
626 two-dimensional triple-quantum MAS ^{11}B NMR. *Solid State Nuclear Magnetic*
627 *Resonance*, 8:109–121, 1997.
- 628 [57] T. Charpentier, J. Virlet. Triple quantum MQMAS spectroscopy of
629 $^{59}Co(I=7/2)$ in $Na_3Co(NO_2)_6$ and *trans*- $Co[(en_2)(NO_2)_2]NO_3$ interplay
630 between the quadrupole coupling and anisotropic shielding tensors. *Solid State*
631 *Nuclear Magnetic Resonance*, 12:227–242, 1998.
- 632 [58] K. Larntz T. Fox, D. Hinkley. Jackknifing in nonlinear regression.
633 *Technometrics*, 22:29–33, 1980.
- 634 [59] B. H. Meier R. R. Ernst T. O. Levante, M. Baldus. Formalized quantum
635 mechanical floquet theory and its application to sample spinning in nuclear
636 magnetic resonance. *Molecular Physics*, 86:1195–1212, 1995.
- 637 [60] D. Massiot P. J. Grandinetti T. Vosegaard, P. Florian. Multiple quantum magic-
638 angle spinning using rotary resonance excitation. *The Journal of Chemical*
639 *Physics*, 114(10):4618–4624, 2001.
- 640 [61] U. Haeberlen, J. S. Waugh. Coherent Averaging Effects in Magnetic Resonance.
641 *Physical Review*, 175:453–467, 1968.
- 642 [62] U. Piantini, O. W. Sorensen, R. R. Ernst. Multiple Quantum Filters for
643 Elucidating NMR coupling Networks. *Journal of the American Chemical*
644 *Society*, 104:6800–6801, 1982.
- 645 [63] M. Wolfsberg V. B. Cheng, H. H. Suzukawa. Investigation of a nonrandom
646 numerical method for multi-dimensional integration. *Journal of Chemical*
647 *Physics*, 59:3992–3998, 1973.
- 648 [64] H. T. Kwak Z. H. Gan. Enhancing mqmas sensitivity using signals from multiple
649 coherence transfer pathways. *Journal of Magnetic Resonance*, 168:346–351,
650 2004.
- 651 [65] P. J. Grandinetti Z. H. Gan. Rotary resonance in multiple-quantum magic-angle
652 spinning. *Chemical Physics Letters*, 352:252–, 2002.
- 653 [66] S. K. Zaremba. Good lattice points, discrepancy, and numerical integration.
654 *Ann. Mat. pura appl.*, 73:293–317, 1966.
- 655 [67] J. W. Zwanziger. Interpreting NMR Spectra of Disordered Materials: Direct
656 Inversion of Powder Patterns. *Solid State Nuclear Magnetic Resonance*, 3:219–
657 229, 1994.